Analysis of Adaptive Digital Feedback Linearization Techniques

Jangheon Kim, *Student Member, IEEE*, Changjoon Park, *Student Member, IEEE*, Junghwan Moon, *Student Member, IEEE*, and Bumman Kim, *Fellow, IEEE*

***Abstract*—A new lookup-table linearization technique is developed based on the digital feedback and digital feedback/predistortion (DFBPD) concepts. The linearization characteristics are investigated through system simulation of a real power-amplifier model with 90-W peak envelope power. The DFB suppresses forward-path nonlinear distortion as a gain reduction due to the FB effect, and this technique enhances the system tolerance without any bandwidth limitation. As the PD network is added to the FB loop, the linearization performance and system tolerance are further improved because of more accurate PD signal extraction. In addition, the gain is purely determined by the FB path, so the gain fluctuation in the forward path, including amplifier aging and temperature effects, is suppressed. The analysis and simulation allow experimental evaluation of the linearization mechanism and performance of the DFBPD technique for an 802.16e mobile Worldwide Interoperability for Microwave Access signal.**

***Index Terms*—Feedback (FB), power amplifier (PA), predistortion (PD), Worldwide Interoperability for Microwave Access (WiMAX).**

I. Introduction

CURRENT AND next-generation wireless communication systems can transmit high-data-rate signals for multimedia communications, including both high- and low-mobility applications such as mobile access, nomadic/local wireless access, etc. The signals of these systems vary rapidly so that they have a wide bandwidth and high peak-to-average power ratio (PAPR), leading to stringent linearity requirements for signal amplification. In addition, power amplifiers (PAs) in the system should be highly efficient as well as highly linear to reduce size and cost of the system. However, it is difficult to simultaneously achieve high efficiency and linearity because the PA design involves a tradeoff. Thus, a linearization technique with low power consumption is desired. The digital predistortion (DPD) technique has been recognized as a promising solution due to its manageable digital operation, low power consumption of the digital part, and powerful linearization ability, so it has been widely studied [1]–[18].

The DPD technique uses linearization algorithms to generate an inverse function of the amplitude and phase distortions, which are described as amplitude-to-amplitude modulation (AM/AM) and amplitude-to-phase modulation (AM/PM). The inverse function is obtained using adaptive algorithms, such as the least mean square, least square (LS), and recursive LS [5], [8], [11]–[15], [19]. Recently, new DPD techniques have been introduced based on feedback (FB) concepts without applying an adaptive algorithm. Chung *et al.* [20] have presented an open-loop Cartesian DPD technique using a lookup table (LUT) for the analog Cartesian FB path. The linearization of this technique is determined by the loop gain of the analog FB path and open-loop gain path. Drawing on the analog FBPD concept [21], our previous works have presented the digital FBPD (DFBPD) technique in terms of the basic concept, operational behavior, system tolerance, and comparison with conventional DPD techniques [22], [23]. This technique operates in two modes: In the noninstantaneous training mode, the LUT of the technique is constructed by the FBPD algorithm, and in the instantaneous operating mode, the system is operated as a function of the input signal in real time, which is like the conventional DPD technique. Thus, the DFBPD technique delivers many advantages such as a simple PD algorithm, fast convergence, accurate PD signal extraction, and good system tolerance because the technique is based on the FB algorithm. Additionally, a wideband DFBPD technique, including a memory-effect compensation algorithm, has been developed to provide good linearization performance for wideband signals [24]. These studies have shown that the DFBPD technique has good connectivity with other linearization architectures, including wideband linearization.

This paper analyzes the linearization mechanisms of the DFBPD technique, which are the PD and FB effects. A DFB algorithm with a large gain reduction (GR) is developed and compared with the FBPD algorithm with and without GR. The linearization performance and system tolerance of each algorithm to amplifier errors are explored through system simulations. Finally, we experimentally evaluate the linearization mechanisms and demonstrate good linearization performance. The DFBPD algorithm enhances the linearity by combining

Manuscript received September 01, 2008; revised January 28, 2009. First published July 14, 2009 ; current version published February 10, 2010. This work was supported in part by the Korean Government under the Korea Science and Engineering Foundation MOST Grant R01-2007-000-20377-0, by the Center for Broadband Orthogonal Frequency Division Multiplex Mobile Access, Pohang University of Science and Technology under the Information Technology Research Center Program of the Korean Ministry of Knowledge Economy, supervised by the Institute for Information Technology Advancement (IITA-2009-C1090-0902-0037), and by the World Class University Program through the Korea Science and Engineering Foundation funded by the Ministry of Education, Science and Technology (Project No. R31-2008-000-10100-0). This paper was recommended by Associate Editor Philip K. T. Mok.

J. Kim is with the Department of Electrical and Computer Engineering, University of Waterloo, Waterloo, ON N2L 3G1, Canada (e-mail: j256kim@engmail.uwaterloo.ca).

C. Park, J. Moon, and B. Kim are with the Department of Electrical Engineering, Pohang University of Science and Technology, Pohang 790-784, Korea (e-mail: tinyhope@postech.ac.kr; jhmoon@postech.ac.kr; bmkim@postech.ac.kr).

Digital Object Identifier 10.1109/TCSI.2009.2027797

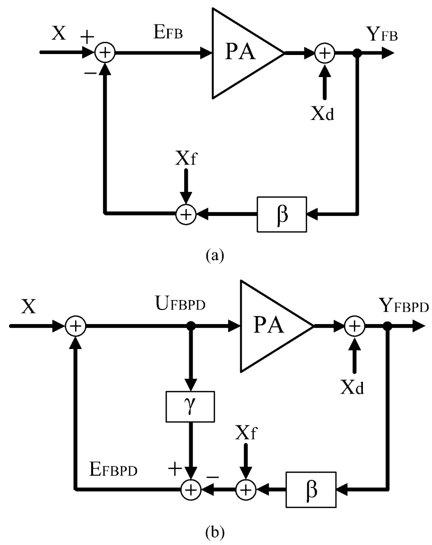

Fig. 1. Simplified block diagram of (a) an FB system and (b) an FBPD system.

FB linearization and PD linearization. Moreover, the system tolerance to forward-path impairments is improved to the level of a pure FB circuit with a very large GR.

II. Operational Behavior and Linearization Mechanisms

A. Analog FB and FBPD Techniques

Fig. 1(a) shows a simplified block diagram of the FB system [7]. In the frequency domain, the input signal X, the FB error signal $E_{\rm FB}$, the distortion of the amplifier X_d, the error of the detection loop X_f, and the output signal $Y_{\rm FB}$ of the system are expressed as

$$E_{\rm FB} = X - (\beta Y_{\rm FB} + X_f) \tag{1}$$

$$Y_{\rm FB} = AE_{\rm FB} + X_d \tag{2}$$

where A is the open-loop gain of the forward path and β is the gain of the FB path. Combining (1) and (2), $E_{\rm FB}$ and $Y_{\rm FB}$ are given by

$$E_{\rm FB} = \frac{X}{1+A\beta} - \frac{\beta X_d}{1+A\beta} - \frac{X_f}{1+A\beta} \tag{3}$$

$$Y_{\rm FB} = \frac{AX}{1+A\beta} + \frac{X_d}{1+A\beta} - \frac{AX_f}{1+A\beta} \tag{4}$$

$$\approx \frac{X}{\beta} + \frac{X_d}{A\beta} - \frac{X_f}{\beta}, \qquad A\beta \gg 1. \tag{5}$$

Fig. 1(b) shows a block diagram of the FBPD system [21]. The operational behavior of the system is not all that different from the FB system. In the frequency domain, the output signal $Y_{\rm FBPD}$ is expressed as

$$Y_{\rm FBPD} = AU_{\rm FBPD} + X_d \tag{6}$$

where

$$U_{\rm FBPD} = X + E_{\rm FBPD} \tag{7}$$

is the input signal to the amplifying element

$$E_{\rm FBPD} = \gamma U_{\rm FBPD} - (\beta Y_{\rm FBPD} + X_f) \tag{8}$$

is the predistorted FB signal, and γ is gain of the signal cancellation path.

From the previous equations, $U_{\rm FBPD}$ and $Y_{\rm FBPD}$ are given by

$$U_{\rm FBPD} = \frac{X}{(1-\gamma)+A\beta} - \frac{\beta X_d}{(1-\gamma)+A\beta} - \frac{X_f}{(1-\gamma)+A\beta} \tag{9}$$

$$Y_{\rm FBPD} = \frac{AX}{(1-\gamma)+A\beta} + \frac{(1-\gamma)X_d}{(1-\gamma)+A\beta} - \frac{AX_f}{(1-\gamma)+A\beta} \tag{10}$$

$$\approx \frac{X}{\beta} + \frac{(1-\gamma)X_d}{A\beta} - \frac{X_f}{\beta}, \qquad A\beta \gg 1$$

$$\equiv \frac{X}{\beta} - \frac{X_f}{\beta}, \qquad \gamma = 1. \tag{11}$$

Equations (5) and (11) clearly describe the behaviors of the two linearization mechanisms. The closed-loop gain of the FB system in (4) approaches the FB loop gain $1/\beta$ only when the loop gain $A\beta \gg 1$. However, the gain of the FBPD system in (10) is $1/\beta$ for any loop gain $A\beta$ when $\gamma = 1$, as well as for large loop gain $A\beta \gg 1$. Since the gain is determined by $1/\beta$, fluctuation in the forward path does not appear at the output. Therefore, the FB systems are independent of PA variation due to temperature drift, supply fluctuation, aging, and so on. The distortion X_d of the FB system is suppressed by an amount equivalent to the GR factor, due to the negative FB effect. The distortion of the FBPD system is suppressed by the FB and the PD effects. However, the distortion can be removed completely, without the help of the FB linearization, by the PD effect with $\gamma = 1$, which represents an accurate error signal extraction and feeding to the amplifier. On the other hand, the error in the FB circuit X_f of either system cannot be suppressed and is forwarded to the output since the gains for X and X_f are identical.

B. DFB and DFBPD Algorithms

In [22], the FBPD architecture and the digital LUT method were combined to create the DFBPD technique. In this paper, the DFB technique is developed to analyze and compare with the linearization mechanisms of the DFBPD technique. The proposed DFB and DFBPD systems are shown in Fig. 2. The gray lines illustrate the FB signal extraction loop as a function of $|(1 + A\beta_{\rm DFB})X_s(n)|$ in Fig. 2(a) and $|A\beta_{\rm DFBPD}X_s(n)|$ in Fig. 2(b), following the circuits in Fig. 1. In these two techniques, the first step is the PA modeling using the input and measured output signals of the amplifier, similar to the conventional DPD technique. The measured open-loop PA characteristic is transformed to a closed-loop system by FB signal injection from the LUT. The training sequence of the LUT is similar to the DPD technique. The LUTs of the systems are slowly adapted. However, the FB signal data in the LUT can be supplied to the system very quickly in real-time operation, delayed only by the

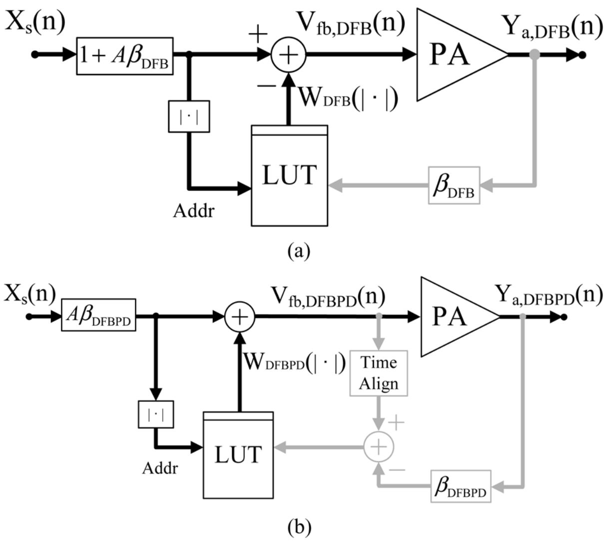

Fig. 2. Simplified block diagram of (a) a DFB system and (b) a DFBPD system. The gray line illustrates the FB signal extraction loop as a function of $|(1 + A\beta_{\rm DFB})X_s(n)|$ and $|A\beta_{\rm DFBPD}X_s(n)|$, respectively, following the circuits in Fig. 1.

data-memory access time. Therefore, the FB technique based on the LUT approach in the digital domain can overcome the bandwidth limitation and eliminate the out-of-band oscillation problem related to the loop delay, which are serious shortcomings of the FB architecture presented in [7], and [25]–[27].

The operating principle of the simplified DFB system block diagram shown in Fig. 2(a) is similar to the analog FB technique described in the previous section. The difference is that, here, the FB signal stored in the LUT is addressed in the digital domain according to the baseband signal. The input drive is increased by $(1 + {\rm A}\beta_{\rm DFB})$ to maintain the same input and output powers. The DFB algorithm consists of the following process. First, it sets the LUT initial value to the zero vector for a training sequence with samples $n = 1, 2, \ldots, N$. Then, the FB signal, which is equal to the amplified source signal, is fed to the amplifier. Next, the FB output signal is stored in the LUT as a function of the input. After storage, the new FB input signal is generated by subtracting the LUT signal from the source signal, and the resultant signal is fed to the amplifier. This process is iterated several times until it converges. This algorithm can be written as

$$\begin{aligned} V_{\rm fb,DFB}^{(k)}(n) &= (1 + A\beta_{\rm DFB})X_s(n) \\ &\quad - W_{\rm DFB}^{(k)}[\theta_{\rm DFB}(n)] \end{aligned} \tag{12}$$

$$\begin{aligned} W_{\rm DFB}^{(k)}[\theta_{\rm DFB}(n)] &= \beta_{\rm DFB} Y_{a,\rm DFB}^{(k-1)}(n)|_{\theta_{\rm DFB}(n)}, \\ &\qquad k = 1, 2, \ldots, K \end{aligned} \tag{13}$$

with

$$\beta_{\rm DFB} = \frac{\delta_{\rm DFB}}{A} \tag{14}$$

$$\theta_{\rm DFB}(n) = |(1 + A\beta_{\rm DFB})X_s(n)| \tag{15}$$

where $V_{\rm fb,DFB}(n)$ is the FB signal, $X_s(n)$ is the input source signal, $W_{\rm DFB}[\theta_{\rm DFB}(n)]$ is the LUT signal, $Y_{a,\rm DFB}(n)$ is the output signal of the DFB system, $\beta_{\rm DFB}$ is the FB path gain, and k is the iteration number. The FB path gain $\beta_{\rm DFB}$ is composed of the open-loop gain of the amplifier A and FB factor $\delta_{\rm DFB}$. The FB signal includes the input signal, out-of-phase distortion signal, and error of the detection loop, as described in (3). The system should have a large GR to improve the distortion-correction capability and system tolerance.

The DFBPD algorithm for the simplified DFBPD system block diagram in Fig. 2(b) is similarly expressed as

$$\begin{aligned} V_{\rm fb,DFBPD}^{(k)}(n) &\\ &= A\beta_{\rm FBPD}X_s(n) + W_{\rm DFBPD}^{(k)}[\theta_{\rm DFBPD}(n)] \end{aligned} \tag{16}$$

$$\begin{aligned} W_{\rm DFBPD}^{(k)}[\theta_{\rm DFBPD}(n)] &\\ &= \left[V_{\rm fb,DFBPD}^{(k-1)}(n) - \beta_{\rm DFBPD}Y_{a,\rm DFBPD}^{(k-1)}(n)\right]|_{\theta_{\rm DFBPD}(n)} \end{aligned} \tag{17}$$

with

$$\beta_{\rm DFBPD} = \frac{\delta_{\rm DFBPD}}{A} \tag{18}$$

$$\theta_{\rm DFBPD}(n) = |A\beta_{\rm DFBPD}X_s(n)| \tag{19}$$

where $V_{\rm fb,DFBPD}(n)$ is the FB signal with PD, $W_{\rm DFBPD}[\theta_{\rm DFBPD}(n)]$ is the LUT signal, $\beta_{\rm DFBPD}$ is the FB path gain, and $\delta_{\rm DFBPD}$ is the FB factor. Here, $W_{\rm DFBPD}[\theta_{\rm DFBPD}(n)]$ is added to the input, similar to the DFB technique. The DFBPD algorithm corrects distortion mainly by the PD effect, with further enhancement by the FB effect. In the digital domain, the algorithm can accurately and quickly compensate the nonlinear characteristics because the cancellation path gain γ term in (10) can be accurately adjusted to one. Moreover, the system becomes immune to PA variation due to temperature drift, supply fluctuation, aging, and so on, because the system gain is independent of the forward-path gain, as described in (11).

In the DFB algorithm, the loop gain $A\beta_{\rm DFB}$ should be increased to properly suppress the distortion; therefore, $\delta_{\rm DFB}$ should be a large value. However, in the training sequence of this algorithm, a $A\beta_{\rm DFB}$ that is greater than one causes an oscillation because the output $Y_{a,\rm DFB}(n)$ depends on the open-loop gain of the measured PA during the first few samples of the transient training sequence. In other words, the algorithm diverges for $\delta_{\rm DFB} \geq 1$, and a stable operation is only possible for

$$0 < \delta_{\rm DFB} < 1. \tag{20}$$

The maximum GR of the DFB algorithm can therefore not exceed 6 dB because the closed-loop voltage gain in (4) is applied for $\delta_{\rm DFB} < 1$ (The closed-loop gain is $20\log_{10}(A/1 + \delta_{\rm DFB})$ from (4) so that the GR value becomes approximately -6 dB for $\delta_{\rm DFB} = 1$). The FB of the DFBPD algorithm is also limited, similar to the DFB algorithm, because the output $Y_{a,\rm DFBPD}(n)$ depends on the open-loop gain of the PA during the first few samples of the training sequence. In the $\delta_{\rm DFBPD} = 1$ case, the gain is not reduced, and the algorithm diverges when $\delta_{\rm DFBPD} \geq 2$. The stability condition is given by

$$1 < \delta_{\rm DFBPD} < 2. \tag{21}$$

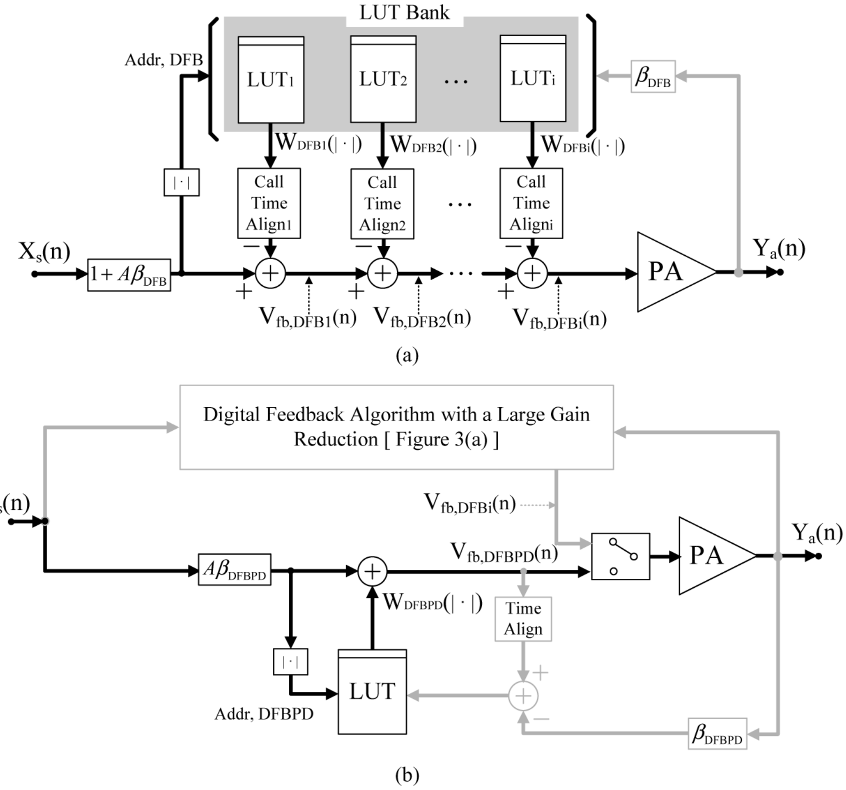

Fig. 3. Simplified block diagram of (a) an iterative DFB algorithm with a large GR and (b) a DFBPD algorithm combined with the iterative DFB algorithm.

The maximum FB amount also cannot exceed 6 dB (The closed-loop gain is $20\log_{10}(A/\delta_{\rm DFBPD})$ from (11) so that the GR value becomes approximately -6 dB for $\delta_{\rm DFBPD}=2$). As a result, the DFB and DFBPD algorithms cannot obtain a large GR value due to the convergence problem. Thus, we propose new DFB and DFBPD algorithms with a large GR of more than 6 dB in the next section.

C. DFB and DFBPD Algorithms With a Large GR

Fig. 3(a) shows a simplified block diagram of the proposed DFB algorithm with a large GR. The limited GR of the DFB algorithm mentioned in the previous section can be overcome by developing an iterative FB algorithm that successively reduces the gain to give a large cumulative GR. During the iterative operation, $\rm LUT_1, LUT_2, \ldots, LUT_i$ in the LUT bank are initialized as zero vectors, and the first DFB algorithm constructs $\rm LUT_1$, maintaining the $\delta_{\rm DFB}<1$ condition of (20). In this process, the FB signal $V_{{\rm fb,DFB}i}(n)$ is equal to $V_{\rm fb,DFB1}(n)$ due to the initial LUT condition, and this signal is fed to the amplifier. In the next step, the FB signal $V_{\rm fb,DFB1}(n)$ of the first FB loop instead of the source signal $X_s(n)$ is applied as the input signal for the second iteration. The second LUT $\rm LUT_2$ is built resulting in a cumulative GR amount of $[1/(1+A\beta_{\rm DFB})]^2$. At the ith iteration, all LUTs are constructed, and the process is continued until the cumulative GR is sufficient. Here, the FB signals $V_{\rm fb,DFB1}(n), V_{\rm fb,DFB2}(n), \ldots, V_{{\rm fb,DFB}i}(n)$ can be written as follows:

$$\begin{aligned}V_{\rm fb,DFB1}^{(k_1)}(n) &= (1+A\beta_{\rm DFB})X_s(n)\\ &\quad - W_{\rm DFB1}^{(k_1)}[\theta_{\rm DFB}(n)]\\ W_{\rm DFB1}^{(k_1)}[\theta_{\rm DFB}(n)] &= \beta_{\rm DFB}Y_{a,\rm DFB1}^{(k_1-1)}(n)|_{\theta_{\rm DFB}(n)},\\ &\qquad k_1=1,2,\ldots,K_1\end{aligned}\tag{22}$$

$$\begin{aligned}V_{\rm fb,DFB2}^{(k_2)}(n) &= V_{\rm fb,DFB1}^{(k_2)}(n)\\ &\quad - W_{\rm DFB2}^{(k_2)}[\theta_{\rm DFB}(n)]\\ W_{\rm DFB2}^{(k_2)}[\theta_{\rm DFB}(n)] &= \beta_{\rm DFB}Y_{a,\rm DFB2}^{(k_2-1)}(n)|_{\theta_{\rm DFB}(n)},\\ &\qquad k_2=K_1+1,K_1+2,\ldots,K_2\end{aligned}\tag{23}$$

$$\vdots$$

$$\begin{aligned}V_{{\rm fb,DFB}i}^{(k_i)}(n) &= V_{{\rm fb,DFB}(i-1)}^{(k_i)}(n)\\ &\quad - W_{{\rm DFB}i}^{(k_i)}[\theta_{\rm DFB}(n)]\\ W_{{\rm DFB}i}^{(k_i)}[\theta_{\rm DFB}(n)] &= \beta_{\rm DFB}Y_{a,{\rm DFB}i}^{(k_i-1)}(n)|_{\theta_{\rm DFB}(n)},\\ &\qquad k_i=K_{i-1}+1,K_{i-1}+2,\ldots,K_i.\end{aligned}\tag{24}$$

The final cumulative GR value becomes $[1/(1+A\beta_{\rm DFB})]^i$, realizing a large GRFB system. As an example, for the iterative DFB algorithm with $\delta_{\rm DFB}=0.9$ and three iteration ($i=3$), the final cumulative GR is about -16.7 dB (the closed-loop gain of this algorithm is $20\log_{10}(A/(1+0.9)^3)$ so that the GR value becomes approximately -16.7 dB).

The successive GR algorithm is also applied to the DFBPD algorithm, as shown in Fig. 3(b). The FB signal of the DFBPD algorithm with the cumulative GR amount of $[1/(1+A\beta_{\rm DFB})]^i$ is given by

$$\begin{aligned}V_{\rm fb,DFBPD}^{(k_{i+1})}(n) &= A\beta_{\rm FBPD}X_s(n) + W_{\rm FBPD}^{(k_{i+1})}[\theta_{\rm DFBPD}(n)]\\ &\qquad k_{i+1}=K_i+1,K_i+2,\ldots,K_{i+1}\end{aligned}\tag{25}$$

where

$$
\begin{aligned}
&W_{\mathrm{DFBPD}}^{(K_i+1)}(\theta_{\mathrm{DFBPD}}(n)) \\
&\quad = [0 \quad 0 \quad 0 \quad \cdots \quad 0 \quad 0]|_{\theta_{\mathrm{DFBPD}}(n)} \\
&W_{\mathrm{DFBPD}}^{(K_i+2)}(\theta_{\mathrm{DFBPD}}(n)) \\
&\quad = \left[V_{\mathrm{fb,DFB}i}^{(K_i+1)}(n) - \beta_{\mathrm{DFBPD}} Y_{a,\mathrm{DFBPD}}^{(K_i+1)}(n)\right]|_{\theta_{\mathrm{DFBPD}}(n)} \\
&W_{\mathrm{DFBPD}}^{(K_i+3)}(\theta_{\mathrm{DFBPD}}(n)) \\
&\quad = \left[V_{\mathrm{fb,DFBPD}}^{(K_i+2)}(n) - \beta_{\mathrm{DFBPD}} Y_{a,\mathrm{DFBPD}}^{(K_i+2)}(n)\right]|_{\theta_{\mathrm{DFBPD}}(n)} \\
&W_{\mathrm{DFBPD}}^{(K_i+4)}(\theta_{\mathrm{DFBPD}}(n)) \\
&\quad = \left[V_{\mathrm{fb,DFBPD}}^{(K_i+3)}(n) - \beta_{\mathrm{DFBPD}} Y_{a,\mathrm{DFBPD}}^{(K_i+3)}(n)\right]|_{\theta_{\mathrm{DFBPD}}(n)} \\
&\quad \vdots \\
&W_{\mathrm{DFBPD}}^{(K_{i+1})}[\theta_{\mathrm{DFBPD}}(n)] \\
&\quad = \left[V_{\mathrm{fb,DFBPD}}^{(K_{i+1}-1)}(n) - \beta_{\mathrm{DFBPD}} Y_{a,\mathrm{DFBPD}}^{(K_{i+1}-1)}(n)\right]|_{\theta_{\mathrm{DFBPD}}(n)}.
\end{aligned}
$$

As indicated in the previous equations, the FB signal includes the PD signal as well as the FB signal with large cumulative GR. As an example, for the DFBPD algorithm with $\delta_{\mathrm{DFBPD}} = 1$ combined with the iterative DFB algorithm with $\delta_{\mathrm{DFB}} = 0.9$ and three iterations ($i = 3$), the cumulative GR is about -16.7 dB, and an accurate FB signal is additionally generated by the PD effect [the closed-loop gain of this algorithm is $20\log_{10}(A/(1+0.9)^3]$ because the FB effect of the algorithm is caused by the iterative DFB algorithm). These algorithms are used to investigate the system performance according to the linearization mechanisms of the adaptive DFB and DFBPD techniques in Sections III and IV.

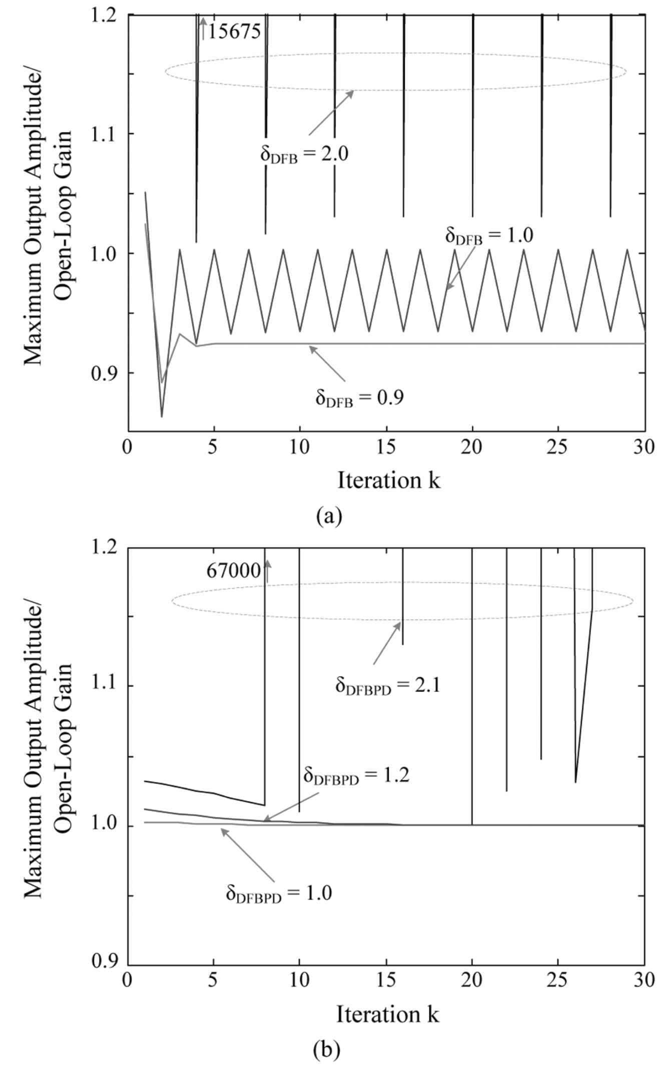

Fig. 4. Simulated convergence characteristics. (a) DFB algorithm. (b) DFBPD algorithm.

III. Simulation Results

System simulations were conducted to investigate the performance of each algorithm. These simulations were based on an equivalent model that includes the nonlinear characteristics and variations of the amplifier and were carried out using MATLAB. For the simulations, a class AB amplifier with low memory effects was implemented using a Freescale MRF5S21090 LDMOS with a 90-W peak envelope power (PEP) [28] and modeled for the AM/AM and AM/PM nonlinear characteristics using the weighted polynomial-function technique [29]. The open-loop gain A of the amplifier was 56.8 dB. The convergence characteristic of the DFB algorithm is shown in Fig. 4(a). Thus, the FB path gains β_{DFB} of the iterative DFB algorithm were adjusted to a δ_{DFB} of 0.9, which means that the successive GRs of the first, second, and third iterations were about 5.6, 11.2, and 16.7 dB, respectively. For the DFBPD algorithm, the convergence characteristic is shown in Fig. 4(b), and δ_{DFBPD} is set to one. The GR was adjusted to either 0 or 16.7 dB. The modulated input signal is an 802.16e mobile Worldwide Interoperability for Microwave Access (WiMAX) signal with a 10-MHz bandwidth and an 8.5-dB PAPR at the 0.01% level of the complementary cumulative distribution function. The algorithms have two LUTs, each with 256 entries for the AM/AM and AM/PM distortions.

A. Linearization Behavior for the FB and FBPD Effects

Error-correction tests for the DFB and DFBPD algorithms were performed for an ideal case with no system error. The predistorted signals for each algorithm, together with the output of the amplifier before correction, are shown in Fig. 5. The signals are predistorted more accurately to suppress the distortion as the gain is decreased. The DFBPD algorithm delivers perfectly predistorted signals for both $\mathrm{GR} = 0$ and 16.7 dB cases. Fig. 6 illustrates the AM/AM and AM/PM characteristics of the amplifier linearized by the algorithms. As the FB effect increases, the AM/AM and AM/PM nonlinear characteristics are reduced. The DFBPD algorithm completely compensates for the AM/AM and AM/PM nonlinear characteristics for both $\mathrm{GR} = 0$ and 16.7 dB. Fig. 7 shows the power spectral densities of the output signals after linearization by the algorithms. The linearization of the DFB algorithms improves as the FB increases. However, high linearity is difficult to achieve using only the FB because of a large gain loss. The DFBPD algorithm can deliver high linearity due to accurate PD without using FB with a large GR, indicating that the PD effect is dominant over the FB effect. The simulation results are summarized in Table I. The adjacent channel leakage

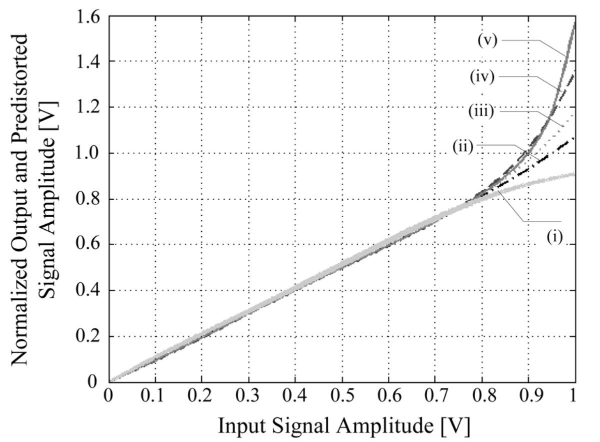

Fig. 5. Simulated output and predistorted signals. (i) Normalized output signal. (ii) DFB signal with 5.6 dB GR. (iii) DFB signal with 11.2 dB GR. (iv) DFB signal with 16.7 dB GR. (v) DFBPD signal with either 0 or 16.7 dB GR.

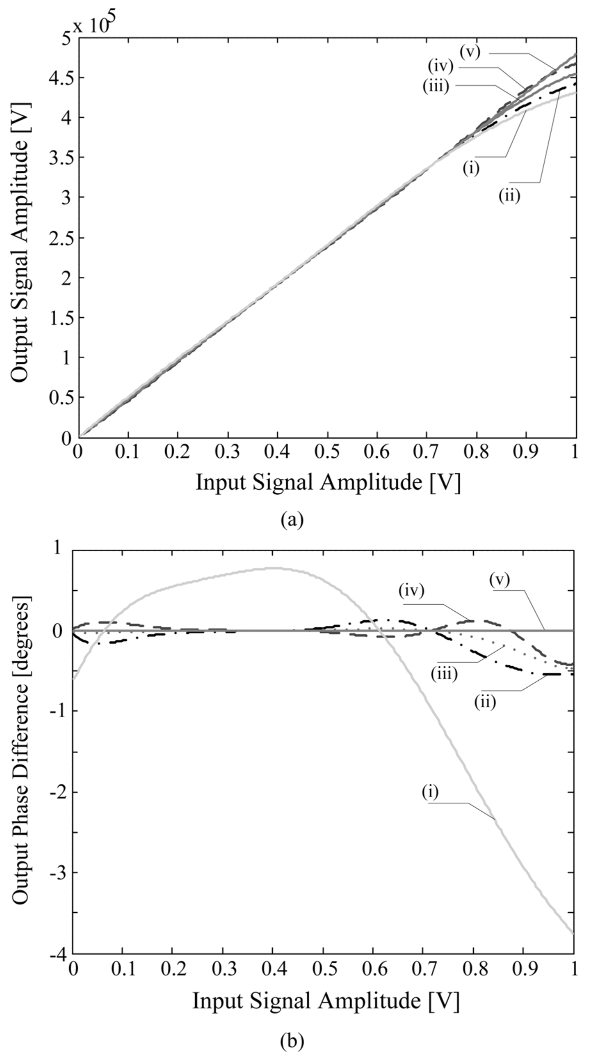

Fig. 6. Simulated (a) AM/AM and (b) AM/PM output characteristics after DFB and DFBPD linearization. (i) Without linearization. (ii) DFB linearization with 5.6 dB GR. (iii) DFB linearization with 11.2 dB GR. (iv) DFB linearization with 16.7 dB GR. (v) DFBPD linearization with either 0 or 16.7 dB GR.

ratio (ACLR) is measured at 7.144-MHz offset, and the relative constellation error (RCE) is $20\log_{10}$(error vector magnitude).

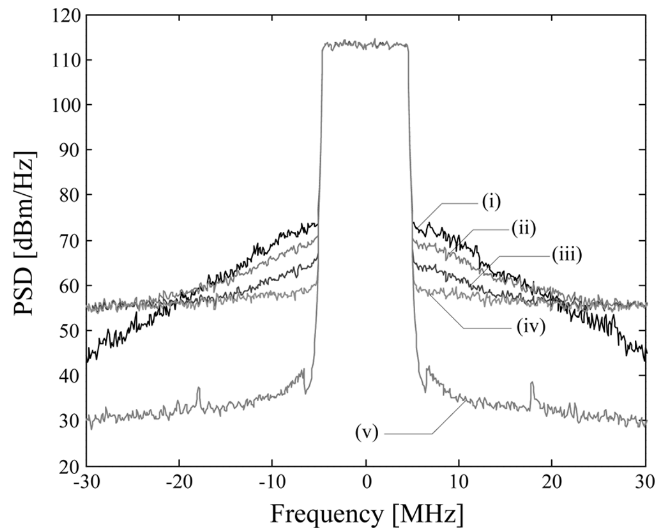

Fig. 7. Simulated 802.16e mobile WiMAX signal spectra before and after linearization. (i) Without linearization. (ii) DFB linearization with 5.6 dB GR. (iii) DFB linearization with 11.2 dB GR. (iv) DFB linearization with 16.7 dB GR. (v) DFBPD linearization with either 0 or 16.7 dB GR.

TABLE I
SIMULATED LINEARIZATION PERFORMANCE FOR AN 802.16E MOBILE WIMAX SIGNAL UNDER IDEAL CONDITIONS

	ACLR [dBc]	RCE [dB]
Amplifier	–42.4	–36.8
DFB with 5.6 dB GR	–47.0	–39.5
DFB with 11.2 dB GR	–50.7	–43.4
DFB with 16.7 dB GR	–54.5	–47.1
DFBPD with 16.7 dB GR	–76.2	–49.1
DFBPD with 0 dB GR	–76.2	–49.1
Signal Source	–76.2	–49.1

B. Effect of Amplifier Variation

As indicated in the previous section, the DFB and DFBPD algorithms can deliver better tolerance to forward-path variations. This is very advantageous because PAs are sensitive to temperature drift, supply fluctuation, amplifier aging, and so on. Thus, the linearization performance was investigated according to the gain variation through system simulations consisting of several steps. First, the DFB and DFBPD algorithms constructed the LUTs before the variation occurred. Nonlinear distortions of the amplifier were linearized by the algorithms, as described in the previous section. Next, the AM/AM and AM/PM nonlinear characteristics of the amplifier were changed to represent the amplifier variation with gain fluctuations of -0.4 and -0.8 dB. When this variation occurred, the linearity of the amplifier degraded for the previous FB signals. Then, the LUTs were adaptively updated for the changed amplifier signals while maintaining the same GR values of the algorithms. Finally, the amplifier was linearized by applying the changed FB signal.

The simulated results are summarized in Tables II and III, which can be compared with the linearization performance in Table I. The gain variations are reduced in the DFB algorithm as the GR is increased. The DFBPD algorithms with and without the GR maintain constant gain, as expected from (11). Moreover, it is shown that the algorithms can operate properly in the

TABLE II
SIMULATED LINEARIZATION PERFORMANCE FOR AN 802.16E MOBILE WIMAX SIGNAL UNDER THE CONDITION OF −0.4 DB GAIN VARIATION

	ACLR [dBc]	RCE [dB]	Gain Fluctuation [dB]
Amplifier	–40.0	–36.8	–0.4
DFB with 5.6 dB GR	–47.0	–39.5	–0.2
DFB with 11.2 dB GR	–50.4	–43.3	–0.2
DFB with 16.7 dB GR	–52.5	–45.2	–0.1
DFBPD with 16.7 dB GR	–75.8	–49.0	0.0
DFBPD with 0 dB GR	–75.8	–49.0	0.0

TABLE III
SIMULATED LINEARIZATION PERFORMANCE FOR AN 802.16E MOBILE WIMAX SIGNAL UNDER THE CONDITION OF −0.8 DB GAIN VARIATION

	ACLR [dBc]	RCE [dB]	Gain Fluctuation [dB]
Amplifier	–39.3	–33.0	–0.8
DFB with 5.6 dB GR	–46.8	–39.0	–0.5
DFB with 11.2 dB GR	–50.0	–43.2	–0.4
DFB with 16.7 dB GR	–52.0	–44.0	–0.3
DFBPD with 16.7 dB GR	–75.0	–49.0	0.0
DFBPD with 0 dB GR	–75.0	–49.0	0.0

face of amplifier variations, although the linearization performance is slightly degraded in the DFB algorithms but not in the DFBPD algorithm. These results indicate that the adaptive DFBPD algorithms are independent of forward-path gain variation and only depend on the FB path gain $1/\beta_{\mathrm{DFBPD}}$, as mentioned in Section II-A, which is a significant advantage for real field applications.

These simulation results show that the adaptive DFBPD algorithm can ideally achieve excellent linearization performance with constant gain in a reasonable PA environment, regardless of the GR factor. In addition, this fact indicates that the PD effect in the DFBPD algorithm is dominant over the FB effect, being capable of achieving good linearization performance in various environments.

IV. EXPERIMENTAL RESULTS

Fig. 8 shows a block diagram of the experimental setup. An Agilent Advanced Design System using an electronic signal generator and vector signal analyzer (ADS-ESG-VSA)-connected solution was used for the test [30]. Linearization by the FB and PD effects of the DFBPD technique were investigated by employing the 802.16e mobile WiMAX signal used in the system simulation. The developed algorithms have two 256-entry AM/AM and AM/PM LUTs, which are programmed in MATLAB using both the DFB and DFBPD algorithms. Here the actual 90-W PA that was modeled in Section III is used, and the linearization capabilities of the algorithms were evaluated only for the memoryless nonlinear characteristics of the amplifier.

Fig. 9 shows the measured amplitude and phase characteristics of the predistorted signals constructed by the DFB and DFBPD algorithms. As described in Section III-A, the input

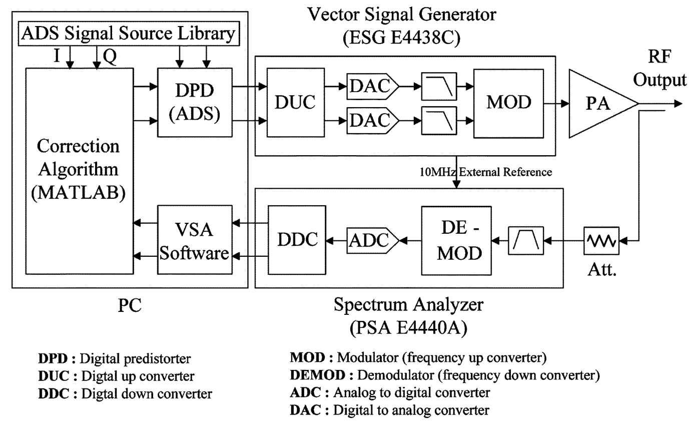

Fig. 8. Block diagram of the experimental setup for linearization test.

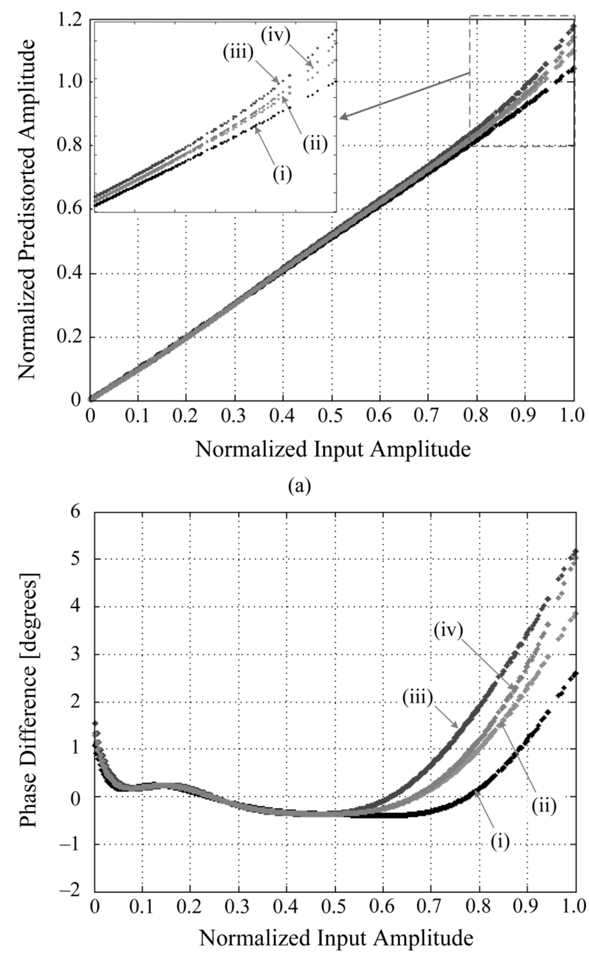

Fig. 9. Measured (a) amplitude and (b) phase characteristics of predistorted signals. (i) DFB linearization with 5.6 dB GR. (ii) DFB linearization with 11.2 dB GR. (iii) DFB linearization with 16.7 dB GR. (iv) DFBPD linearization with either 0 or 16.7 dB GR.

signal levels are adjusted by the GR factor of the DFB algorithm to get the same output power, and the error signal is negatively fed back to cancel the distortion of the amplifier. The predistorted input signal is further expanded for a large GR in Fig. 9(a). The predistorted signals generated by the DFBPD algorithm with 0 or 16.7 dB GR factor are identical, and they are the perfect

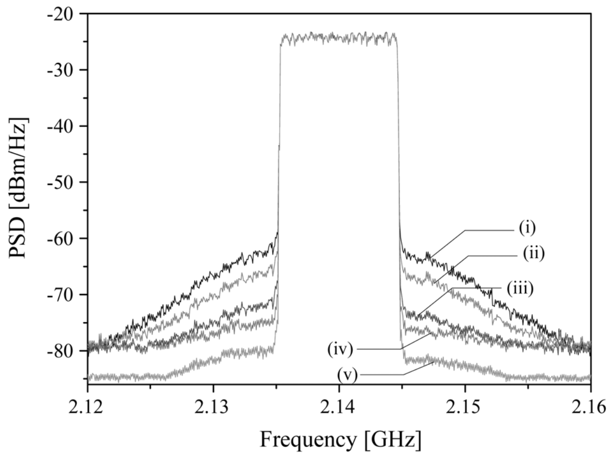

Fig. 10. Measured 802.16e mobile WiMAX signal spectra before and after the successive DFB and DFBPD linearizations. (i) Without the linearization. (ii) DFB linearization with 5.6 dB GR. (iii) DFB linearization with 11.2 dB GR. (iv) DFB linearization with 16.7 dB GR. (v) DFBPD linearization with either 0 or 16.7 dB GR.

PD signals to linearize the amplifier distortion. Fig. 10 shows the measured output signal spectra for the predistorted signals at an average output power of 40 dBm. The out-of-band distortion is further suppressed by increasing the GR factor of the DFB algorithm. The ACLR at an offset of 7.144 MHz for the DFB algorithm with 16.7 dB GR is −51.6 dBc, which is an improvement of 13 dB. The ACLR with the DFBPD algorithm with or without GR is −56.5 dBc, an improvement of 17.9 dB. Fig. 11 shows the measured constellation diagram of the 802.16e WiMAX signal at the same average output power. The in-band distortion is also further suppressed by increasing the GR factor of the DFB algorithm. The RCE for the DFB algorithm with 16.7 dB GR is −44.3 dB, and for the DFBPD case, is −45.9 dB, which is an improvement of 11.9 dB. The measurement results are summarized in Tables IV and V.

The experimental results show that the DFBPD algorithm can successfully linearize nonlinear distortion, following the analysis described in Sections II and III. The powerful linearization capability is due mainly to the PD effect, and the FB effect can be ignored due to the accurate error extraction.

V. Conclusion

This paper has analyzed the linearization mechanism of the DFBPD technique, which is based on FB and PD effects, and has compared it with the DFB technique. The DFB technique follows the well-known linearization performance of analog FB. The DFBPD algorithm can create a perfect PD signal without the help of the FB effect, providing a powerful linearization. Moreover, the gain of the DFBPD algorithm only depends on the FB path gain, suppressing amplifier-gain fluctuations caused by temperature variation or aging. This is a significant advantage in real field operations. The linearization effects have been tested using a class AB amplifier with 90-W PEP. Increasing the gain factor improves the linearization of the in-band and out-of-band distortion of an 802.16e mobile WiMAX signal; the DFB algorithm with 16.7 dB GR has an ACLR and RCE of −51.6 dBc and −44.3 dB, respectively, at an average output power of 40 dBm. The FBPD algorithm delivers better linearization performance, with an ACLR of −56.5 dBc and RCE of −45.9 dB at the same average output power. We conclude from the simulation and experimental results that the PD effect of the DFBPD algorithm can deliver a good linearization performance with high system

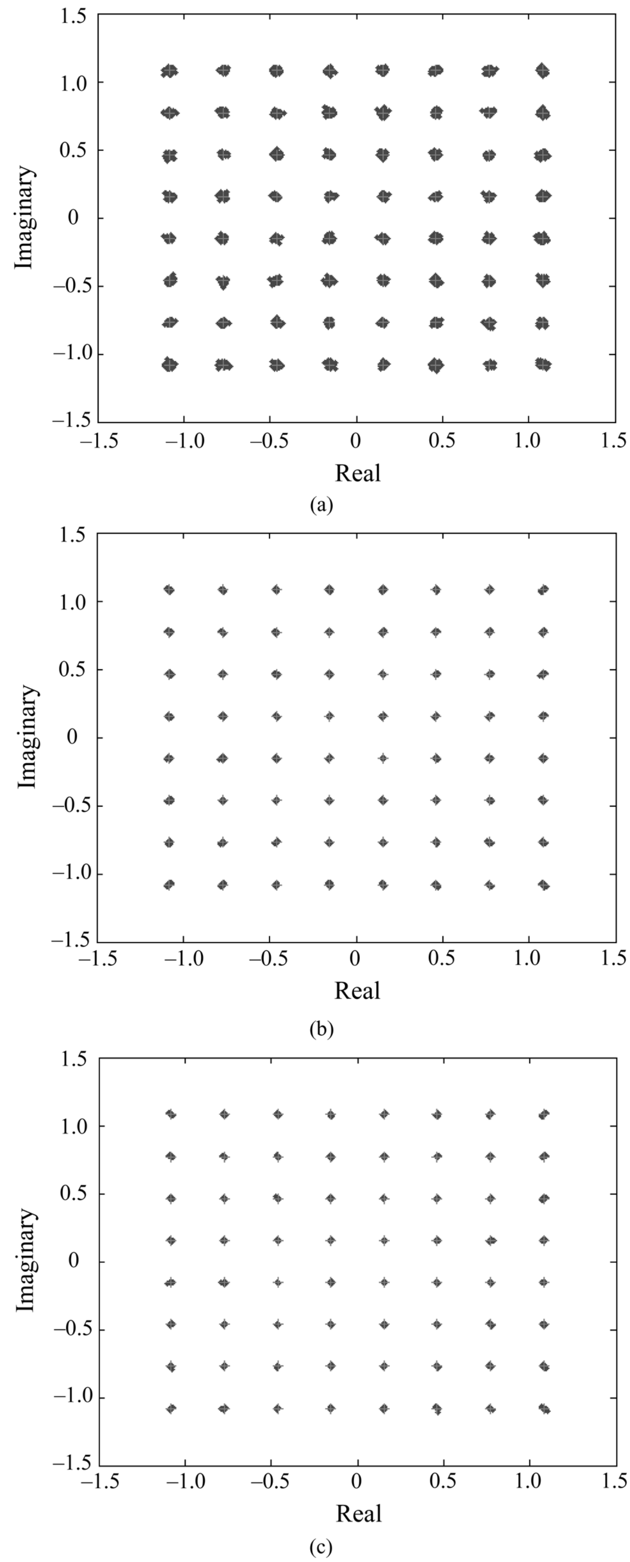

Fig. 11. Measured constellation diagrams. (a) Without linearization. (b) DFB linearization with 16.7 dB GR. (c) DFBPD linearization with either 0 or 16.7 dB GR.

TABLE IV
MEASURED LINEARIZATION PERFORMANCE AT AN AVERAGE OUTPUT POWER OF 40 DBM FOR AN 802.16E MOBILE WIMAX SIGNAL

	ACLR [dBc] at –/+ 7.144 MHz	RCE [dB]
Amplifier	–38.6 /–39.7	–34.0
DFB with 5.6 dB GR	–42.3 /–43.3	–37.6
DFB with 11.2 dB GR	–48.3 /–49.8	–42.7
DFB with 16.7 dB GR	–51.6 /–52.8	–44.3
DFBPD with 16.7 dB GR	–56.5 /–58.3	–45.9
DFBPD with 0 dB GR	–56.5 /–58.3	–45.9

TABLE V
PERFORMANCE COMPARISON BETWEEN DFB AND DFBPD TECHNIQUES AT AN AVERAGE OUTPUT POWER OF 40 DBM FOR AN 802.16E MOBILE WIMAX SIGNAL

	DFB	DFBPD
Linearization Mechanism	FB	FB and PD
GR Amount	16.7 dB	0 dB or 16.7 dB
ACLR Improvement	13.0 dB	17.9 dB
RCE Improvement	10.3 dB	11.9 dB

tolerance. We believe that the DFBPD algorithm without any GR is a very useful and powerful technique for linearizing current and next-generation base-station transmitters.

ACKNOWLEDGMENT

The authors would like to thank the Telecommunication Research and Development Center, Samsung Electronics Company Ltd., for supplying the 802.16e mobile WiMAX signal used in this study. The authors would also like to thank the reviewers for their valuable comments and, particularly, for extensive editing of this paper.

REFERENCES

[1] Y. Nagata, "Linear amplification techniques for digital mobile communications," in *Proc. IEEE 39th Veh. Technol. Conf.*, 1989, pp. 159–164.

[2] J. K. Cavers, "Amplifier linearization using a digital predistorter with fast adaptation and low memory requirements," *IEEE Trans. Veh. Technol.*, vol. 39, no. 4, pp. 374–382, Nov. 1990.

[3] A. S. Wright and W. G. Durtler, "Experimental performance of an adaptive digital linearized power amplifier," *IEEE Trans. Veh. Technol.*, vol. 41, no. 4, pp. 395–400, Nov. 1992.

[4] M. Faulkner and M. Johansson, "Adaptive linearization using predistortion—Experimental results," *IEEE Trans. Veh. Technol.*, vol. 43, no. 2, pp. 323–332, May 1994.

[5] C. Eun and E. J. Powers, "A new Volterra predistorter based on the indirect learning architecture," *IEEE Trans. Signal Process.*, vol. 45, no. 1, pp. 223–227, Jan. 1997.

[6] F. Antonio, W. Hamdy, P. Heidmann, J. Heizer, N. Kasturi, D. P. Osés, and C. Riddle, "A novel adaptive predistortion technique for power amplifiers," in *Proc. IEEE 49th Veh. Technol. Conf.*, May 1999, pp. 1505–1509.

[7] P. B. Kenington, *High-Linearity RF Amplifier Design*. Norwood, MA: Artech House, 2000.

[8] S. Takabayashi, M. Orihashi, T. Matsuoka, and M. Sagawa, "Adaptive predistortion linearizer with digital quadrature modem," in *Proc. IEEE 51st Veh. Technol. Conf.*, May 2000, pp. 2237–2241.

[9] K. J. Muhonen, M. Kavehrad, and R. Krishnamoorthy, "Lookup table techniques for adaptive digital predistortion: A development and comparison," *IEEE Trans. Veh. Technol.*, vol. 49, no. 9, pp. 1995–2002, Sep. 2000.

[10] F. H. Raab, P. Asbeck, S. Cripps, P. B. Kenington, Z. B. Popovic, N. Pothecary, J. F. Sevic, and N. O. Sokal, "Power amplifiers and transmitters for RF and microwave," *IEEE Trans. Microw. Theory Tech.*, vol. 50, no. 3, pp. 814–826, Mar. 2002.

[11] L. Ding, G. T. Zhou, D. R. Morgan, Z. Ma, J. S. Kenney, J. Kim, and C. R. Giardina, "A robust digital baseband predistorter constructed using memory polynomials," *IEEE Trans. Commun.*, vol. 52, no. 1, pp. 159–165, Jan. 2004.

[12] K. Horiguchi, M. Miki, J. Nagano, H. Senda, K. Yamauchi, M. Nakayama, and T. Takagi, "A UHF-band digital pre-distortion power amplifier using weight-divided adaptive algorithm," in *Proc. IEEE MTT-S Int. Microw. Symp. Dig.*, 2004, pp. 2019–2022.

[13] L. Ding, Z. Ma, D. R. Morgan, M. Zierdt, and J. Pastalan, "A least-squares/Newton method for digital predistortion of wideband signals," *IEEE Trans. Commun.*, vol. 54, no. 5, pp. 833–840, May 2006.

[14] H.-H. Chen, C.-H. Lin, P.-C. Huang, and J.-T. Chen, "Joint polynomial and lookup-table predistortion power amplifier linearization," *IEEE Trans. Circuits Syst. II, Exp. Briefs*, vol. 53, no. 8, pp. 612–616, Aug. 2006.

[15] S. D. Muruganathan and A. B. Sesay, "A QRD-RLS-based predistortion scheme for high-power amplifier linearization," *IEEE Trans. Circuits Syst. II, Exp. Briefs*, vol. 53, no. 10, pp. 1108–1112, Oct. 2006.

[16] H. Koeppl and P. Singerl, "An efficient scheme for nonlinear modeling and predistortion in mixed-signal systems," *IEEE Trans. Circuits Syst. II, Exp. Briefs*, vol. 53, no. 12, pp. 1368–1372, Dec. 2006.

[17] L. Ding, Z. Ma, D. R. Morgan, M. Zierdt, and G. T. Zhou, "Compensation of frequency-dependent gain/phase imbalance in predistortion linearization systems," *IEEE Trans. Circuits Syst. I, Reg. Papers*, vol. 55, no. 1, pp. 390–397, Jan. 2008.

[18] M. M. Sahbany and P. P. G. Gulak, "Efficient compensation of the nonlinearity of solid-state power amplifiers using adaptive sequential Monte Carlo methods," *IEEE Trans. Circuits Syst. I, Reg. Papers*, vol. 55, no. 10, pp. 3270–3283, Nov. 2008.

[19] S. Haykin, *Adaptive Filter Theory*. Upper Saddle River, NJ: Prentice-Hall, 2001.

[20] S. Chung, J. W. Holloway, and J. L. Dawson, "Open-loop digital predistortion using Cartesian feedback for adaptive RF power amplifier linearization," in *Proc. IEEE MTT-S Int. Microw. Symp. Dig.*, Jun. 2007, pp. 1449–1452.

[21] Y. Kim, Y. Yang, S. Kang, and B. Kim, "Linearization of 1.85-GHz amplifier using feedback predistortion loop," in *Proc. IEEE MTT-S Int. Microw. Symp. Dig.*, 1998, pp. 1675–1678.

[22] Y. Y. Woo, J. Kim, J. Yi, S. Hong, I. Kim, J. Moon, and B. Kim, "Adaptive digital feedback predistortion technique for linearizing power amplifiers," *IEEE Trans. Microw. Theory Tech.*, vol. 55, no. 5, pp. 932–940, May 2007.

[23] Y. Y. Woo, J. Kim, S. Hong, I. Kim, J. Moon, J. Yi, and B. Kim, "A new adaptive digital predistortion technique employing feedback technique," in *Proc. IEEE MTT-S Int. Microw. Symp. Dig.*, Jun. 2007, pp. 1445–1448.

[24] J. Kim, Y. Y. Woo, J. Moon, and B. Kim, "A new wideband adaptive digital predistortion technique employing feedback linearization," *IEEE Trans. Microw. Theory Tech.*, vol. 56, no. 2, pp. 385–392, Feb. 2008.

[25] M. Johansson and T. Mattsson, "Transmitter linearization using Cartesian feedback for linear TDMA modulation," in *Proc. IEEE 39th Veh. Technol. Conf.*, May 1991, pp. 439–444.

[26] J. L. Dawson and T. H. Lee, "Automatic phase alignment for a fully integrated Cartesian feedback power amplifier system," *IEEE J. Solid-State Circuits*, vol. 38, no. 12, pp. 2269–2279, Dec. 2003.

[27] S. Pipilos, Y. Papananos, N. Naskas, M. Zervakis, J. Jongsma, T. Gschier, N. Wilson, J. Gibbins, B. Carter, and G. Dann, "A transmitter IC for TETRA systems based on a Cartesian feedback loop linearization technique," *IEEE J. Solid-State Circuits*, vol. 40, no. 3, pp. 707–718, Mar. 2005.

[28] J. Cha, I. Kim, S. Hong, B. Kim, J. S. Lee, and H. S. Kim, "Memory effect minimization and wide instantaneous bandwidth operation of a base station power amplifier," *Microw. J.*, vol. 50, no. 1, pp. 66–82, Jan. 2007.

[29] S. Hong, Y. Y. Woo, J. Kim, J. Cha, I. Kim, J. Moon, J. Yi, and B. Kim, "Weighted polynomial digital predistortion for low memory effect Doherty power amplifier," *IEEE Trans. Microw. Theory Tech.*, vol. 55, no. 5, pp. 925–931, May 2007.

[30] *"Connected Simulation and Test Solutions Using the Advanced Design System,"* Agilent Technol., Palo Alto, CA, 2000, Applicat. Note 1394.

Jangheon Kim (S'07) received the B.S. degree in electronics and information engineering from Chonbuk National University, Chonju, Korea, in 2003 and the Ph.D. degree in electrical engineering from the Pohang University of Science and Technology (POSTECH), Pohang, Korea, in 2009.

He is currently a Postdoctoral Fellow with the University of Waterloo, Waterloo, ON, Canada. His current research interests include highly linear and efficient RF PA design, memory-effect compensation techniques, digital predistortion (DPD) techniques, and wideband and high-power RF amplifiers.

Dr. Kim is the recipient of the Highest Efficiency Award at the Student High-Efficiency Power Amplifier Design Competition in the IEEE MTT-S International Microwave Symposium (IMS), 2008.

Changjoon Park (S'07) received the B.S. degree from the Department of Materials Science and Electronic and Electrical Engineering, Pohang University of Science and Technology (POSTECH), Pohang, Korea, in 2003 and the Ph.D. degree in the Department of Electronic Engineering, POSTECH, in 2010.

His current research interests include digital RF systems, CMOS RF circuits for wireless communications, and mixed-mode signal processing IC design.

Junghwan Moon (S'07) received the B.S. degree in electrical and computer engineering from the University of Seoul, Seoul, Korea, in 2006 and is currently working toward the Ph.D. degree at the Pohang University of Science and Technology (POSTECH), Pohang, Korea.

His current research interests include highly linear and efficient RF PA design, memory-effect compensation techniques, digital predistortion (DPD) techniques for linearizing high-power RF amplifiers, and efficiency-improvement techniques.

Mr. Moon is the recipient of the Highest Efficiency Award at the Student High-Efficiency Power Amplifier Design Competition in the IEEE MTT-S International Microwave Symposium (IMS), 2008.

Bumman Kim (M'78–SM'97–F'07) received the Ph.D. degree in electrical engineering from Carnegie Mellon University, Pittsburgh, PA, in 1979.

From 1978 to 1981, he was engaged in fiber-optic network component research with GTE Laboratories Inc., Waltham, MA. In 1981, he was with the Central Research Laboratories, Texas Instruments Incorporated, Dallas, where he was involved in development of GaAs power field-effect transistors (FETs) and monolithic microwave integrated circuits (MMICs). He has developed a large-signal model of a power FET, dual-gate FETs for gain control, high-power distributed amplifiers, and various millimeter-wave MMICs. Since 1989, he has been with the Pohang University of Science and Technology (POSTECH), Pohang, Korea, where he is a Namko Professor with the Department of Electrical Engineering, and Director of the Microwave Application Research Center, where he is involved in device and circuit technology for RF integrated circuits (RFICs). He was a Visiting Professor of electrical engineering with the California Institute of Technology, Pasadena, in 2001. He has authored over 250 technical papers.

Dr. Kim is a member of the Korean Academy of Science and Technology and the Academy of Engineering of Korea. He was an Associate Editor of the IEEE TRANSACTIONS ON MICROWAVE THEORY AND TECHNIQUES and a distinguished Lecturer of the IEEE Microwave Theory and Techniques Society (IEEE MTT-S).